

Existence and Azimuthal Modulational Stability of Vortices in the Cubic-Quintic Nonlinear Schrödinger Equation

R. M. Caplan

May 27, 2009

Abstract

We study the existence and azimuthal modulational stability of vortices in the two-dimensional Cubic-Quintic Nonlinear Schrödinger Equation (CQNLS).

Our method to find the vortex solutions is to use an asymptotically derived trial function in a variational approach and seeding the resulting ansatz as an initial condition to a numerical nonlinear optimization routine. Existence bounds of the vortices are also explored.

We study the azimuthal modulational stability of the vortices by freezing the radial direction of the Lagrangian functional of the CQNLS in order to form a quasi-one dimensional azimuthal equation of motion. A stability analysis is then done in Fourier space of the azimuthal modes, and the results are analyzed using both the asymptotic variational approach ansatz and numerically-exact vortices. For unstable vortices, predictions are given for the growth rates of the most unstable azimuthal mode. We also give predictions for the critical value of the complex frequency, above which all vortices are azimuthally stable.

Our predictions are compared with results found in other publications, as well as against our own full two-dimensional simulations of the vortices.

1 Introduction

The Cubic-Quintic Nonlinear Schrödinger Equation (CQNLS) can be used to model a variety of physical systems. Some examples include light propagation through nonlinear optical media such as double-doped optical fibers [1] and non-Kerr crystals [2]. The key feature of CQNLS models is the competition of the focusing and defocussing nonlinear terms. This allows for the existence of stable structures which would otherwise be unstable in the cubic NLS.

Our present work investigates the azimuthal stability of vortex solutions to the CQNLS. Vortices are ring-shaped structures which have a rotational periodic angular phase associated with them. The number of such periods in a vortex is referred to as its ‘charge’, denoted as m . It is well known that both the cubic NLS and the CQNLS can support vortices [3]. An example of a vortex is depicted in Fig. 1. In the cubic NLS, all vortex solutions are azimuthally unstable, meaning that their structure breaks down in the azimuthal direction into a number of filaments [4]. In contrast to this, the CQNLS can support azimuthally stable vortices [3], in addition to unstable ones. An example of azimuthal break up of a vortex is given in Fig. 2.

There has been numerous studies of the azimuthal stability of the vortices in the CQNLS [3], [5], [6], [7], [8]. Specifically, the studies try to find the critical value of the complex frequency (denoted as Ω) above which all vortices (for a specific charge) are stable. However, the results of the different studies do not agree with each other.

In Ref. [3], azimuthally stable vortices of charge $m = 1$ were shown to exist. Later in Refs. [5], [6], and [7], it was shown that stable vortex solutions exist for vortices of charge 1 and 2, but not for any larger charges. In [8], it is shown theoretically that stable vortices exist for *all* charges, but that the stability region (i.e. the values of Ω between the critical value and the existence bound) in which the solutions reside shrinks

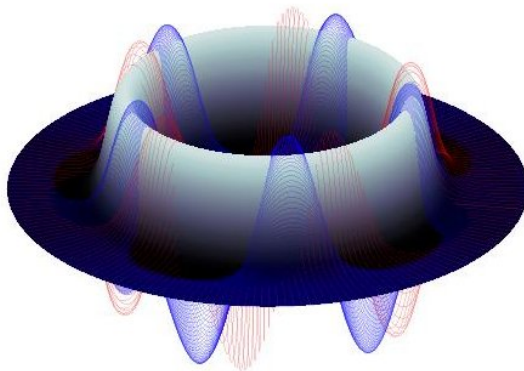


Figure 1: Depiction of a simulated two-dimensional vortex of charge $m = 5$ and complex frequency $\Omega = 0.16$ in the CQNLS. The apparent ‘height’ of the vortex represents the value of the wave function. The gray area represents the modulus-squared, while the blue and red meshes are the real and imaginary parts respectively.

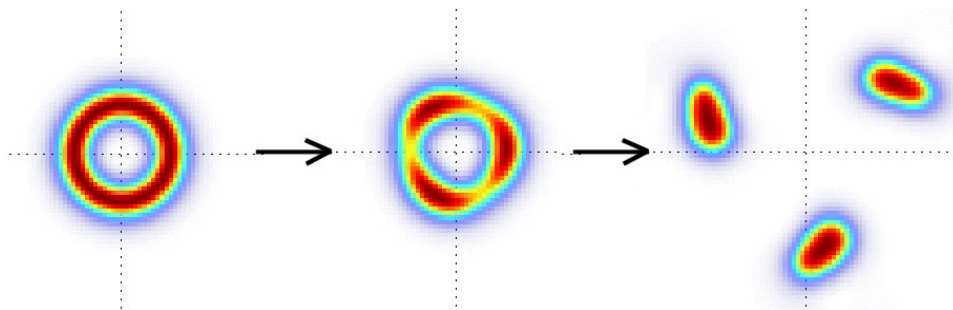


Figure 2: Example of a simulated vortex of charge $m = 4$ in the CQNLS exhibiting break up over time (left to right) due to azimuthal modulational instability. Shown is the intensity depicted by the modulus-squared of the wave-function. Numerical methods and parameters are consistent with those described in Sec. 6.

rapidly with increasing charge. In all the studies, predictions of the critical value of Ω are made for different charges, but each study state different values.

In our present work, we plan to use the methodology from our previous research [4] to study the azimuthal modulational stability (AMS) of vortices in the CQNLS, in an effort to corroborate and compare our results with those in the aforementioned studies. In the process we also are able to predict the growth rates of unstable vortices.

In the process of our analysis, we also formulate analytic expressions (using a variational approach (VA)) for the vortex solution profiles which are extremely close to the true profiles. From these analytic profiles, we are able to derive analytic expressions for azimuthal stability criteria. We also use our VA ansatz to confirm the existence bounds of the vortex solutions.

Obtaining azimuthally stable vortices for numerous charges would have bearing on the prospect of using optical vortices propagating in nonlinear media as a form of data compression. For example, if the stability window shrinks too rapidly, forming vortices in the stability region would become exceedingly experimentally difficult. Knowing the growth rates of unstable modes is also important in this context because if the rates are small enough, then the vortices could be considered ‘quasi-stable’ in that they will not exhibit noticeable instability over the propagation distance required by the physical experiment.

2 Cubic-Quintic NLS and Vortex Solutions

We start with a general representation of the CQNLS with no external potential term:

$$ia \frac{\partial \phi}{\partial \tau} + b \left(\frac{\partial^2 \phi}{\partial X^2} + \frac{\partial^2 \phi}{\partial Y^2} \right) + \tilde{c} |\phi|^2 \phi + \tilde{d} |\phi|^4 \phi = 0, \quad (1)$$

where ϕ is the wave function, τ is the propagation dimension, X and Y are the transverse directions, and a , b , \tilde{c} , and \tilde{d} are parameters determined by the physical system. In order to simplify the analysis, we write the parameters on the nonlinearities as $s_1 c$ and $s_2 d$ where $c = |\tilde{c}|$, $d = |\tilde{d}|$, and $s_1, s_2 \in [\pm 1]$ are the signs of \tilde{c} and \tilde{d} respectively.

We can non-dimensionalize Eq. (1) without loss of generality by applying the following rescalings:

$$\begin{aligned} \phi &= \alpha \Psi, & X &= \beta x, \\ \tau &= \gamma t, & Y &= \beta y, \end{aligned} \quad (2)$$

which, after dividing through Eq. (1) by α , yields:

$$ia \frac{1}{\gamma} \frac{\partial \Psi}{\partial t} + b \frac{1}{\beta^2} \left(\frac{\partial^2 \Psi}{\partial x^2} + \frac{\partial^2 \Psi}{\partial y^2} \right) + s_1 c \alpha^2 |\Psi|^2 \Psi + s_2 d \alpha^4 |\Psi|^4 \Psi = 0. \quad (3)$$

If we set our rescalings to be:

$$\gamma = \frac{ad}{c^2}, \quad \beta^2 = \frac{bd}{c^2}, \quad \alpha^2 = \frac{c}{d}, \quad (4)$$

we obtain the non-dimensionalized CQNLS:

$$i\Psi_t + \nabla^2 \Psi + s_1 |\Psi|^2 \Psi + s_2 |\Psi|^4 \Psi = 0, \quad (5)$$

where $\nabla^2 \Psi$ is the two-dimensional Laplacian of the wave function. Since the natural coordinate system for studying vortices is polar, the Laplacian takes on the well-known form:

$$\nabla^2 \Psi = \frac{1}{r} \frac{\partial}{\partial r} \left(r \frac{\partial \Psi}{\partial r} \right) + \frac{1}{r^2} \frac{\partial^2 \Psi}{\partial \theta^2}. \quad (6)$$

The CQNLS can support bright vortices when $s_1 = +1$ and $s_2 = -1$ [3]. A steady state vortex is described in general as:

$$\Psi(r, \theta, t) = f(r) e^{i(m\theta + \Omega t)}, \quad (7)$$

where $f(r) \in \mathfrak{R}$ is the steady state radial profile, m is the topological charge, and Ω is the complex frequency. Finding $f(r)$ profiles for different values of m and Ω is not trivial, and has no analytical solution available. In addition, the profile $f(r)$ does not exist for certain values of Ω as will be discussed in Sec. 3.4.

We begin our study by finding approximate analytic expressions for $f(r)$ and studying their existence bounds.

3 Approximate Analytical Steady State Vortex Profiles

In this section, we develop an approximate analytical solution to the CQNLS vortex profile. Our profile is very close to the true solution (as will be shown in Sec. 4.3), and therefore can be used to predict existence regions and make analytical AMS predictions.

3.1 Review of One-Dimensional Steady-State Profile

Before tackling the 2D vortices' radial profile, we first review the steady state profile solution to the one-dimensional CQNLS. This one-dimensional profile will be used as an ansatz for a variational approach to find two-dimensional radial profiles in Sec. 3.3.

The non-dimensionalized one-dimensional CQNLS takes the form:

$$i\Psi_t + \Psi_{xx} + |\Psi|^2\Psi - |\Psi|^4\Psi = 0, \quad (8)$$

while the one-dimensional steady state profile takes the form:

$$\Psi(x, t) = f(x) e^{i\Omega t}. \quad (9)$$

When Eq. (9) is inserted into Eq. (8), we get the following ordinary differential equation (ODE):

$$-\Omega f(x) + \frac{d^2 f}{dx^2} + f^3(x) - f^5(x) = 0. \quad (10)$$

Eq. (10) can be solved for $f(x)$, which yields a soliton-like profile [9]:

$$f^2(x) = \frac{4\Omega}{1 + \sqrt{1 - (16/3)\Omega} \cosh(2\sqrt{\Omega} x)}. \quad (11)$$

It should be noted that this is not a true soliton, but rather a quasi-soliton as solutions of the form of Eq. (11) exhibit inelastic collisions [9]. It is apparent that the solution does not exist for all values of Ω . The maximum value that Ω can take is:

$$\Omega_{\max}^{1D} = 3/16 = 0.1875. \quad (12)$$

Therefore, there is an existence region of $\Omega \in [0, \Omega_{\max}^{1D}]$, where when $\Omega = \Omega_{\max}^{1D}$, the solution is simply a constant value of $f(x) = f_0 = \sqrt{3/4}$, and $\Omega = 0$ yields the trivial solution. This solution describes a sech-shaped curve which flattens out as $\Omega \rightarrow \Omega_{\max}^{1D}$. The family of solutions is depicted in Fig.3.

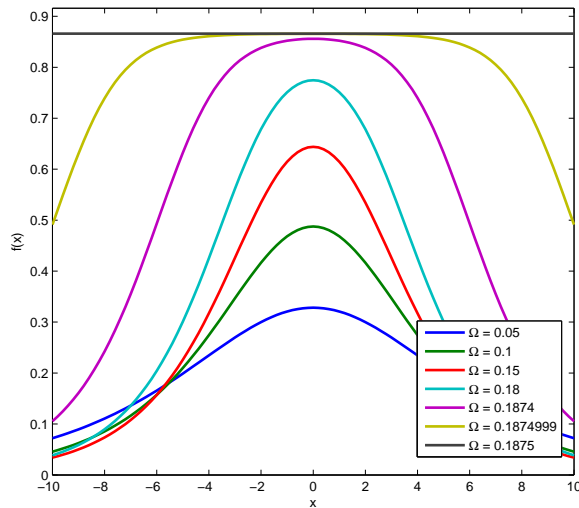


Figure 3: Depictions of steady state solitary solutions for the one-dimensional CQNLS for various values of Ω . We see that as Ω increases, the profile starts to flatten out. At the critical value, it becomes constant valued.

3.2 Asymptotic Two-Dimensional CQNLS Vortex Profile

From our previous work in Ref. [4], we found that for the cubic NLS, by assuming certain asymptotic approximations, the ODE describing a two-dimensional steady state vortex profile became equivalent to a modified version of the one-dimensional ODE describing a steady state profile solution. This allows one to use the one-dimensional profile solution as an ansatz to a variational approach to find an approximate analytical two-dimensional vortex profile. Our goal in this section is to show that the same situation holds true for the CQNLS.

We start by inserting the general form of a vortex as described in Eq. (7) into the two-dimensional CQNLS of Eq. (5) to yield the following ODE:

$$-\left(\Omega + \frac{m^2}{r^2}\right) f(r) + \frac{1}{r} \frac{d}{dr} \left(r \frac{df}{dr} \right) + f^3(r) - f^5(r) = 0. \quad (13)$$

If we assume that the vortex has a large radius, then the region of interest in the evolution equation has $r \gg 1$, in which case the variations in the variable r behave like a constant (denoted r_c), which we take to be the center of the radial profile. With this assumption, Eq. (13) becomes:

$$-\left(\Omega + \frac{m^2}{r_c^2}\right) f(r) + \frac{d^2 f}{dr^2} + f^3(r) - f^5(r) = 0, \quad (14)$$

which is exactly the same form as the one-dimensional CQNLS profile ODE described by Eq. (10). The difference is that here, we have an offset Ω value. We designate this offset Ω as:

$$\Omega^* = \Omega + \frac{m^2}{r_c^2}, \quad (15)$$

and can then rewrite Eq. (14) as:

$$-\Omega^* f(r) + \frac{d^2 f}{dr^2} + f^3(r) - f^5(r) = 0. \quad (16)$$

The steady state profile for Eq. (16) is simply the same as the one-dimensional case (whose center position is offset by r_c)

$$f_{\text{asy}}^2(r) = \frac{4\Omega^*}{1 + \sqrt{1 - (16/3)\Omega^*} \cosh\left(2\sqrt{\Omega^*}(r - r_c)\right)}. \quad (17)$$

What we need now is an expression for the central radius of the profile, r_c , and the shifted frequency, Ω^* . Finding one of the two automatically gets us the other from the expression in Eq. (15). In Sec. 3.3, we will use a variational approach to find the parameters r_c and Ω^* . Before doing that, we first glean some information directly from Eq. (17).

If we assume Ω to be very near the two-dimensional existence bound Ω_{max}^{2D} , we can get an expression for the amplitude of the profile at $\Omega = \Omega_{\text{max}}^{2D}$. We do this by setting $f(r) \equiv f_0$ in Eq. (14), where f_0 is a constant (remembering that the profile at the existence bound is constant valued) that satisfies

$$-\left(\Omega + \frac{m^2}{r_c^2}\right) f_0 + f_0^3 - f_0^5 = 0. \quad (18)$$

Solving Eq. (18) for f_0 yields:

$$f_0^2 = \frac{1}{2} \left[1 \pm \sqrt{1 - 4 \left(\Omega + \frac{m^2}{r_c^2} \right)} \right]. \quad (19)$$

At $\Omega = \Omega_{\text{max}}^{2D}$, Eq. (19) is equal to the amplitude of Eq. (17). By setting $r = r_c$ in Eq. (17), we know the maximum value of $f_{\text{asy}}(r)$ is:

$$f_{\text{max}}^2 = \frac{4 \left(\Omega + \frac{m^2}{r_c^2} \right)}{1 + \sqrt{1 - (16/3) \left(\Omega + \frac{m^2}{r_c^2} \right)}} \quad (20)$$

Setting Eq. (20) to be equal to Eq. (19) we can solve for r_c and we get:

$$r_c^{\text{asy}} = \frac{m}{\sqrt{\frac{3}{16} - \Omega}}. \quad (21)$$

This expression for the vortex radius r_c is only valid at $\Omega = \Omega_{\text{max}}^{2\text{D}}$ (which, as we will see is equal to $3/16$, making the radius infinite), but can be useful to get a quick approximation of the radius of vortices that have Ω very close to $\Omega_{\text{max}}^{2\text{D}}$.

We also notice that if we insert Eq. (21) into Eq. (20) with $\Omega = \Omega_{\text{max}}^{2\text{D}}$, we find that, like in the one-dimensional profile, the amplitude at the existence bound is:

$$f_0^2 = 3/4. \quad (22)$$

3.3 Variational Approach

In this section we will use a variational approach to find our approximate vortex profile. We start by inserting the general vortex solution of Eq. (7) into the Lagrangian density of the CQNLS:

$$\mathcal{L}(r, \theta) = \left(\Omega + \frac{m^2}{r^2} \right) f(r)^2 + \left(\frac{df}{dr} \right)^2 - \frac{1}{2} f(r)^4 + \frac{1}{3} f(r)^6. \quad (23)$$

Since $f(r)$ is a steady state, the radial integrals over $f(r)$ in the Lagrangian will become constants (which will depend on m and Ω), and so we can write the Lagrangian as:

$$L = 2\pi \left(\Omega C_1 + m^2 C_3 + C_2 - \frac{1}{2} C_4 + \frac{1}{3} C_5 \right), \quad (24)$$

where:

$$\begin{aligned} C_1 &= \int_0^\infty f^2(r) r dr, & C_2 &= \int_0^\infty \left(\frac{df}{dr} \right)^2 r dr, & C_3 &= \int_0^\infty \frac{1}{r^2} f^2(r) r dr, \\ C_4 &= \int_0^\infty f^4(r) r dr, & C_5 &= \int_0^\infty f^6(r) r dr. \end{aligned} \quad (25)$$

We now need to insert an ansatz into the Lagrangian. We choose our ansatz to be our asymptotic approximate profile of Eq. (17), where we will treat Ω^* and r_c as our variational parameters. Inserting Eq. (17) into the C -constant integrals of the Lagrangian, and using the same large radius approximations described in Ref. [10] yields:

$$\begin{aligned} C_1 &\approx 2\sqrt{3} T r_c, \\ C_2 &\approx r_c \left[\frac{3}{9} \sqrt{\Omega^*} - \sqrt{3} T \left(\frac{3}{16} - \Omega^* \right) \right], \\ C_3 &\approx \frac{2\sqrt{3} T}{r_c}, \\ C_4 &\approx -3 r_c \left[\sqrt{\Omega^*} - \frac{\sqrt{3}}{2} T \right], \\ C_5 &\approx -r_c \left[\frac{27}{8} \sqrt{\Omega^*} - \sqrt{3} T \left(\frac{27}{16} - 3\Omega^* \right) \right], \end{aligned} \quad (26)$$

where:

$$T = \operatorname{arctanh} \left[\sqrt{\frac{3}{16\Omega^*}} - \sqrt{\frac{3}{16\Omega^*} - 1} \right], \quad (27)$$

The Euler-Lagrangian equations take the form

$$\frac{\partial L}{\partial \Omega^*} = 0, \quad \frac{\partial L}{\partial r_c} = 0. \quad (28)$$

Evaluating Eq. (28) leads to two equations for Ω^* and r_c . Solving the equations we get

$$r_c^{\text{va}} = m \left[\Omega - \frac{3}{16} + \frac{1}{2T} \sqrt{\frac{3}{16} \Omega^*} \right]^{-1/2}, \quad (29)$$

$$\Omega^* = \Omega + \frac{m^2}{(r_c^{\text{va}})^2},$$

where T is as defined in Eq. (27).

We cannot write an explicit analytical closed form for r_c in terms of Ω since Eq. (29) is transcendental. However, it is possible to solve for r_c numerically using a root finder routine, and then using the result to obtain the desired VA profile.

Our asymptotic variational ansatz (denoted VA) is now:

$$f_{\text{va}}^2(r) = \frac{4\Omega^*}{1 + \sqrt{1 - (16/3)\Omega^*} \cosh\left(2\sqrt{\Omega^*}(r - r_c)\right)}, \quad (30)$$

where r_c and Ω^* are determined by Eq. (29).

There is a nice analytical result that can be obtained from Eq. (29) without the need to use root-finder numerical methods. If we combine the two equations, we can rearrange terms to get an analytical form for Ω as a function of Ω^* :

$$\Omega = G(\Omega^*) = \frac{\Omega^*}{2} + \frac{3}{32} - \frac{1}{4T} \sqrt{\frac{3}{16} \Omega^*}, \quad (31)$$

and we can write r_c in terms of $G(\Omega^*)$ as

$$r_c^{\text{va}} = \frac{m}{\sqrt{\Omega^* - G(\Omega^*)}}, \quad (32)$$

which is simply a rearrangement of Eq. (15). With this formulation of the VA, we can easily see how Ω and Ω^* are related, as well as how r_c^{va} behaves. It should be noted, that it seems that while r_c^{va} depends on m , the relationship between Ω and Ω^* does not. In Fig. 4 we show r_c^{va} versus Ω and Ω^* with $m = 5$. We see that as one increases Ω (and Ω^*), the radius of the vortex starts out very large (infinity for $\Omega = 0$), decreases until it reaches a minimum value, and then increases rapidly (it becomes infinite once again at $\Omega = \Omega_{\text{max}}^{\text{2D}}$).

3.4 Existence Bounds for Two-Dimensional Vortex Profiles

From numerical investigations done in Refs. [3] and [11], the value of the existence criteria for a 2D CQNLS vortex solution was stated as $\Omega_{\text{max}}^{\text{2D}} \approx 0.180$. Later it was shown analytically in Ref. [8] that:

$$\Omega_{\text{max}}^{\text{2D}} = \Omega_{\text{max}}^{\text{1D}} = 3/16 = 0.1875. \quad (33)$$

The numerical discrepancy can possibly be explained by looking at the relationship between Ω and Ω^* found through the variational approach given by Eq. (31). From Eq. (31) and Eq. (27), we see that as $\Omega^* \rightarrow 0.1875$, $T \rightarrow \infty$, and so $\Omega = G(\Omega^*) \rightarrow \Omega^*/2 + 3/32 = 0.1875$. This confirms that $\Omega_{\text{max}}^{\text{2D}} = \Omega_{\text{max}}^{\text{1D}} = 0.1875$. In Fig. 5 we plot $\Omega = G(\Omega^*)$ versus Ω^* for $\Omega^* \in [0.01, 0.1875]$. We see that as $\Omega^* \rightarrow 0.1875$, $\Omega \rightarrow 0.1875$, but appears to only get to around 0.171 before jumping to 0.1875. The reason for this ‘jump’ is due to the extreme sensitivity of the relationship between Ω and Ω^* near $\Omega_{\text{max}}^{\text{2D}}$. In Table. 1 we show some example values of Ω^* and the corresponding $G(\Omega^*) = \Omega$. As is clearly seen, one quickly approaches the limit of machine precision

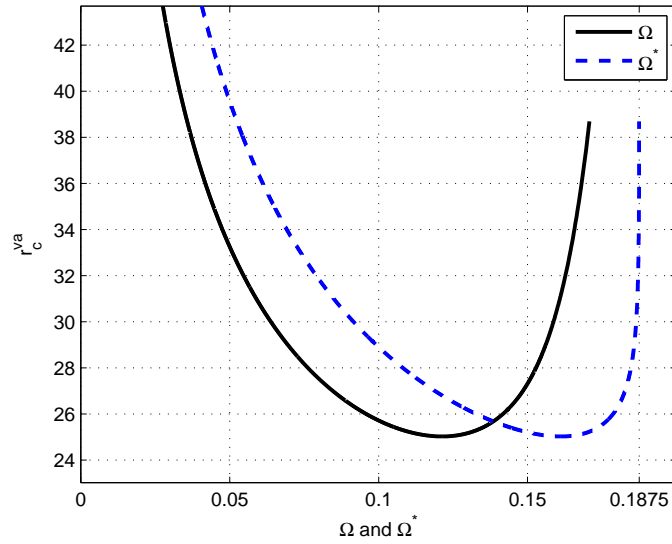


Figure 4: The vortex radius of our VA ansatz r_c^{va} versus $\Omega = G(\Omega^*)$ and Ω^* for charge $m = 5$.

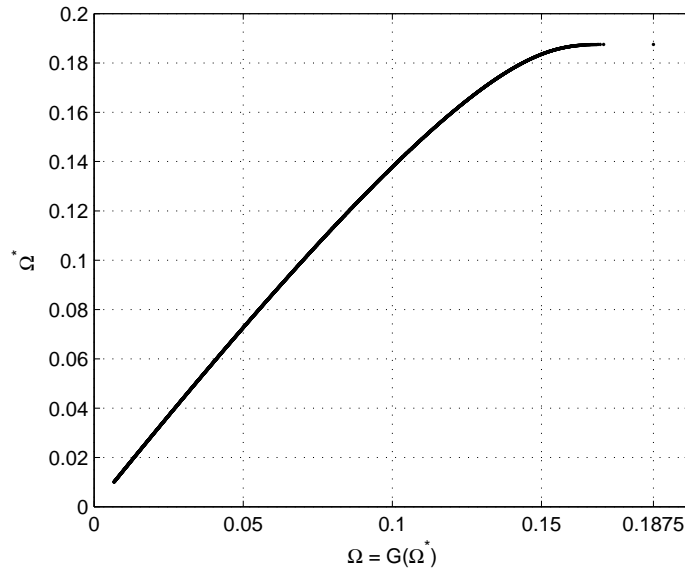


Figure 5: The values of $\Omega = G(\Omega^*)$ vs. Ω^* from our VA ansatz. The relationship is independent of the charge m . We see that $\Omega \rightarrow 0.1875$ as $\Omega^* \rightarrow 0.1875$. We evaluate $G(\Omega^*)$ over an interval of $\Omega^* \in [0.01 : 0.00001 : 0.1875]$.

Table 1: Evaluation of $\Omega = G(\Omega^*)$ near 0.1875. We only show four significant digits on $G(\Omega^*)$. The extreme sensitivity of the relationship is easily observed.

Ω^*	$\Omega = G(\Omega^*)$
0.1874	0.1664
0.187499	0.1736
0.187499999	0.1783
0.187499999999	0.1806
0.187499999999999	0.1823

in Ω^* as $\Omega \rightarrow 0.1875$. It is not surprising then, that numerical estimates of Ω_{\max}^{2D} (done by using a shooting method to try to find profiles at different Ω values) gave lower estimates of the existence bound. In Sec. 4.2, we confirm that the existence bound of Ω_{\max}^{2D} is greater than the numerical estimates of Refs. [3] and [11] by finding numerically exact vortex profiles with $\Omega > 0.180$.

Now that we have our analytical approximations to the vortex profile, we need to refine them numerically into the true profile solutions.

4 Numerically-Exact Steady State Vortex Profiles

In order to find numerically-exact profile solutions, we use a nonlinear optimization routine. After describing the method and showing results, we compare our VA profile to our numerically-exact profiles.

4.1 Numerical Nonlinear Optimization

We recall that the goal is to find the radial profile $f(r)$ which satisfies Eq. (13) for a given m and Ω . If we discretize the radial direction and use a second order finite difference approximation for the derivatives, we can write Eq. (13) as a vector function:

$$\vec{F}(\vec{f}(r)) = - \left(\Omega + \frac{m^2}{r_i^2} \right) f_i + \frac{1}{r_i} \frac{1}{\Delta r} \left(r_{i+\frac{1}{2}} \frac{f_{i+1} - f_i}{\Delta r} - r_{i-\frac{1}{2}} \frac{f_i - f_{i-1}}{\Delta r} \right) + f_i^3 - f_i^5 = \vec{0}, \quad (34)$$

where Δr is the radial grid spacing length, $r_i = i\Delta r$, and $f_i = f(r_i)$.

We want a discrete radial profile input vector (\vec{f}^*) which satisfies $\vec{F}(\vec{f}^*) = \vec{0}$. We solve this minimization problem using a numerical optimization algorithm known as the modified Gauss-Newton method (GN) [12].

We iterate a trial solution (\vec{f}_0) of Eq. (34) towards a local minimum solution, \vec{f}^* , by taking steps defined as

$$\vec{f}_{k+1} = \vec{f}_k + \alpha_k \vec{p}_k,$$

where α_k is the step length and \vec{p}_k is the step direction for step number k .

To mark our progress towards $\vec{F}(\vec{f}^*(r)) = \vec{0}$ we define a merit function as

$$M(\vec{f}) = \frac{1}{2} \sum_{i=1}^n (F_i(\vec{f}))^2. \quad (35)$$

This merit function is useful because its gradient is easily computed as

$$\nabla M(\vec{f}) = J(\vec{f})^T \vec{F}(\vec{f}), \quad (36)$$

which is needed in computing α_k at each step. This is done by using an inexact line search along the step direction (\vec{p}_k) (using backtracking search) in order to satisfy a minimum ‘progress’ condition. The progress condition we use is:

$$M(f_k + \alpha_k p_k) \leq M(f_k) + c_1 \alpha_k \nabla M_k^T p_k, \quad (37)$$

where $0 < c_1 < 1$ [12], and is referred to as the first Wolfe condition. It guarantees that we will find a satisfactory step length for each iteration.

To determine the step direction we use the modified Gauss-Newton step:

$$\vec{p}_k = -(J_k^T J_k + \Lambda_k I)^{-1} J_k^T \vec{F}(f_k), \quad (38)$$

where J_k is the Jacobian of \vec{f}_k and Λ_k is called the forcing term. The forcing term is needed because during our iterations it is possible that we end up near a local minimum where $\nabla M(f_k) = 0$, but $M(\vec{f}^*) \neq 0$. This would cause the line search to give $\alpha_k = 0$, and cause $J_k^T J_k$ to become singular, which in turn causes the classic Gauss-Newton step to become undefined. Modifying the GN by adding the forcing term prevents this by ensuring $(J_k^T J_k + \Lambda_k I)$ is not singular.

Choosing the value for Λ_k is not trivial. If the value is too high, then the step direction becomes closer to the steepest decent direction (since as $\Lambda_k \rightarrow \infty$, $p_k \rightarrow -J_k^T \vec{F}(f_k)$), and fast convergence is lost. If the value for Λ_k is too small, then near non-zero roots of M , the length of each step becomes very small, and fast convergence is lost. Through experimentation, we find that a fixed value of $\Lambda_k = 0.0001 \forall k$ works well for our problem [12].

Our stopping criterion is when $M(\vec{f}) < \epsilon_{\text{GM}}$, where ϵ_{GM} is our tolerance. Typically we set this to be between 10^{-8} and 10^{-4} .

4.2 Numerical Steady-State Profile Results

In Fig. 6, we show some radial profiles computed with our GN routine for various values of Ω with charges $m = 1$ and $m = 5$. We show some profiles with $\Omega > 0.180$ including some with values of Ω as high as $\Omega = 0.1874$ which is consistent with the existence bound of $\Omega_{\text{max}}^{\text{2D}} = 0.1875$ reported in Ref. [8] and predicted by our variational approach. We see that independent of charge, as Ω grows, the profiles flatten out and seem to converge to a constant width of around 50. Further increases in Ω push the profile farther out from $r = 0$, but do not seem to change the width or height.

To confirm that the profile solutions we compute from the GN routine are true steady state vortex solutions, we use them as initial conditions to our full two-dimensional simulation of the CQNLS and run them for a very long time. After numerous simulations, we confirm that the GN profiles are steady states.

4.3 Comparison Between VA and Numerically-Exact GN Vortex Profiles

Here we show the accuracy our VA ansatz by comparing it to the numerically exact solutions computed with the GN routine. In Fig. 7 we compare the vortex central radius r_c between the VA and GN profiles for $\Omega \in [0.05, 0.17]$. and $m = 5$. We also plot the radius computed from the asymptotic expression of Eq. (21). We see that the asymptotic radius converges to the true radius as $\Omega \rightarrow \Omega_{\text{max}}^{\text{2D}}$. We also see that the radius of the VA and GN are extremely close allowing one to use the VA radius as an accurate prediction of the true radius of a vortex (something that could be useful in experimental situations).

To get a better idea of how close the VA is to the GN profile overall, in Fig. 8 we compare the relative sum of squares error between our VA profiles and the numerically exact GN profiles for different charges and different values of Ω . We see that as the charge increases, the error between the VA and the GN profiles decreases. The total error is also observed to be quite low, showing that our VA profile is an extremely close description of the true profile.

Since our VA is very accurate we can justifiably use it to compute AMS predictions (see Sec. 5.3).

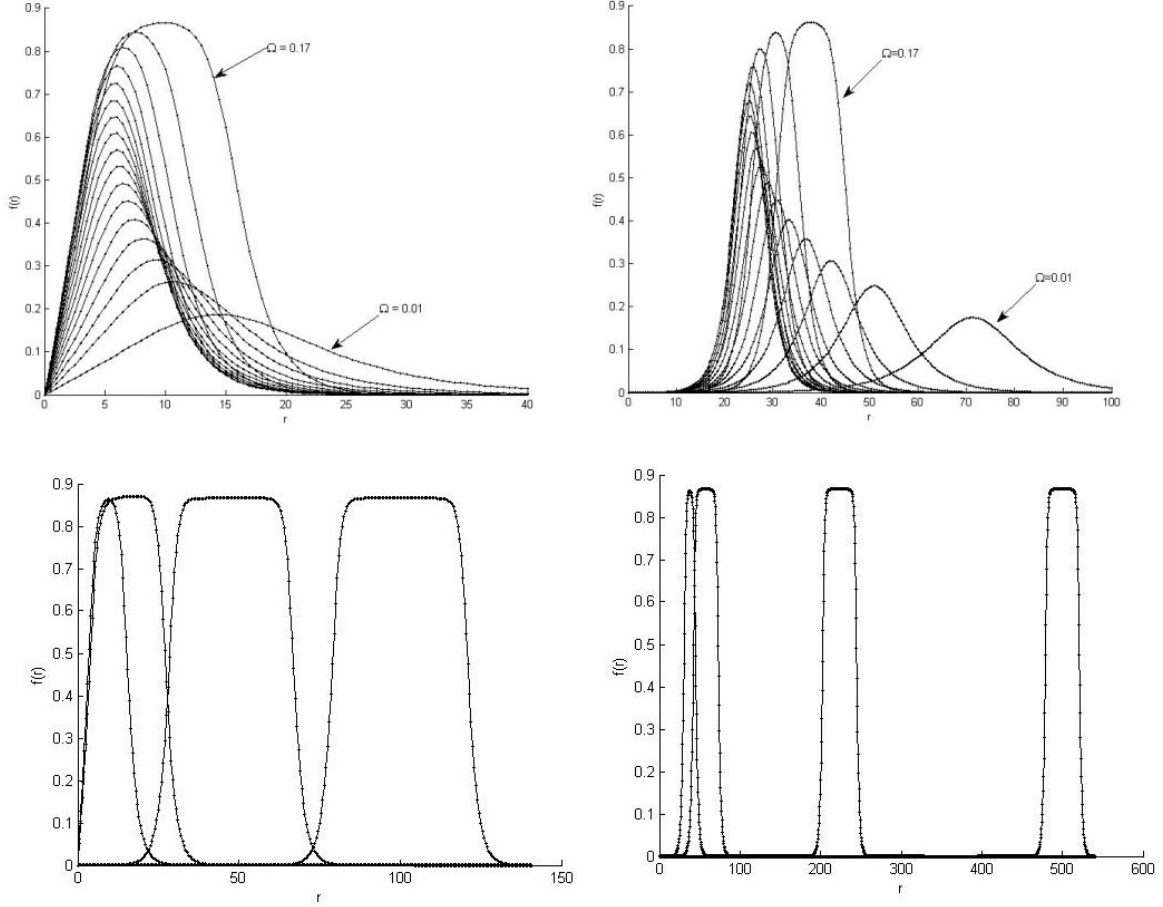


Figure 6: Steady state vortex radial profiles computed with the GN routine for various values of Ω . Left column: $m = 1$, Right column: $m = 5$. The top profiles have a range of $\Omega \in [0.01, 0.17]$ with $\Delta\Omega = 0.01$, while the bottom profiles have $\Omega = [0.170, 0.180, 0.1870, 0.1874]$. For all profiles we used our VA ansatz as an initial condition (not shown). We used $\Delta r = 0.5$ and a stopping tolerance of 10^{-4} . We see that independent from the charge, as Ω grows, the profiles flatten out and seems to converge to a constant width of around 50.

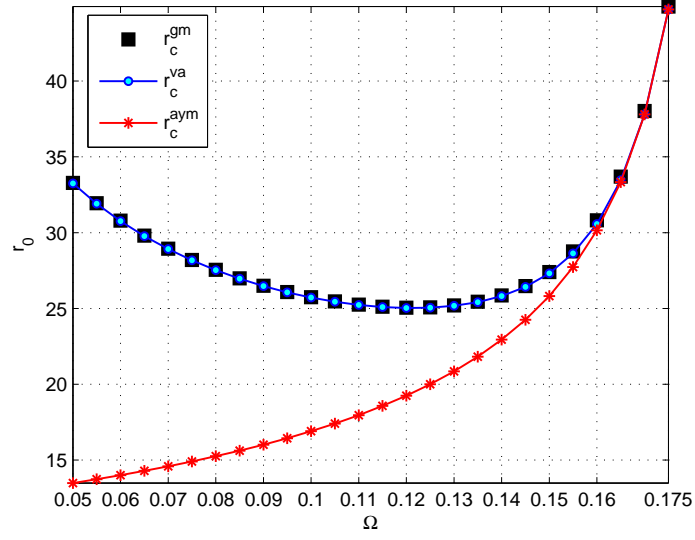


Figure 7: The value of the central vortex radius r_c versus Ω for our VA profile, GN profile, and the asymptotic approximation of Eq. (21). We have set $\Delta r = 0.5$, $m = 5$, and $\Omega \in [0.05, 0.175]$. We see that the VA and GN are extremely close, and that the asymptotic radius converges to the true radius as $\Omega \rightarrow \Omega_{\max}^{2D}$.

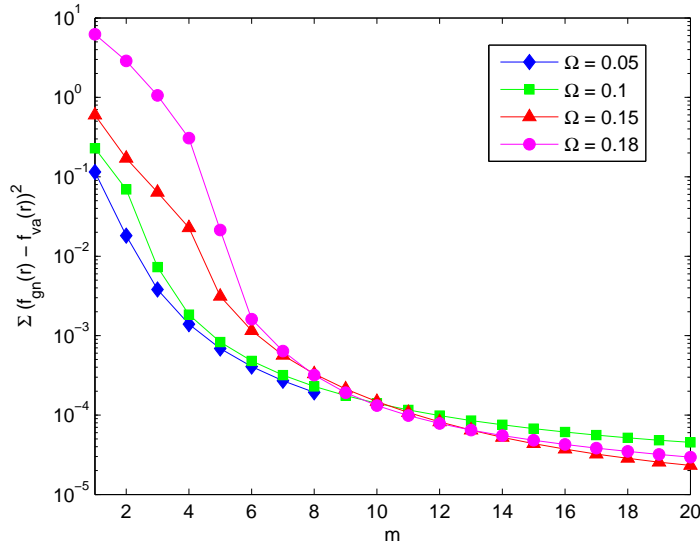


Figure 8: Sum of squares error between our VA vortex profile and the numerically-exact profiles computed with our GN routine. We have set $\Delta r = 0.5$ and the GN tolerance to 10^{-6} . We see that the error decreases as m increases. The error values for $\Omega = 0.1$ stop at $m = 8$ because at that point the VA profiles are already within tolerance of the GN routine.

5 Azimuthal Modulational Stability - Analytic Theory

Now that we can find steady state vortices to the two dimensional CQNLS, we can study their azimuthal modulational stability (AMS). We repeat for the CQNLS, the methodology utilized in our previous work for the cubic NLS [4]. We derive an azimuthal equation of motion by assuming a frozen radial profile, and then perform a perturbation analysis on it to predict the stability of azimuthal perturbation modes.

5.1 Azimuthal Equation of Motion

We start with the Lagrangian Density of the CQNLS given by Eq. (5):

$$\mathcal{L} = \frac{i}{2} (\Psi \Psi_t^* - \Psi^* \Psi_t) + |\Psi_r|^2 + \frac{1}{r^2} |\Psi_\theta|^2 - \frac{s_1}{2} |\Psi|^4 - \frac{s_2}{3} |\Psi|^6. \quad (39)$$

To find the azimuthal equation of motion, we assume a separable time-dependent solution with a steady-state (i.e. ‘frozen’) radial profile:

$$\Psi(r, \theta, t) = f(r) A(\theta, t), \quad (40)$$

where all of the phase components of the solution are contained in A , and therefore $f(r) \in \mathfrak{R}$.

We should note, that it was shown in Ref. [4] that assuming such separability for the evolution of a vortex is not precise, and can lead to discrepancy between the AMS predictions and the numerical results. Still, it was postulated that as one increases the charge m , the predictions made assuming separability increase in their accuracy towards the true results. With this in mind, we proceed with our analysis.

Inserting Eq. (40) into Eq. (39) yields:

$$\mathcal{L} = f^2(r) \frac{i}{2} (AA_t^* - A^* A_t) + \left(\frac{df}{dr} \right)^2 |A|^2 + \frac{1}{r^2} f^2(r) |A_\theta|^2 - f^4(r) \frac{s_1}{2} |A|^4 - f^6(r) \frac{s_2}{3} |A|^6. \quad (41)$$

To compute the Lagrangian, one must integrate the Lagrangian density over all space. Since our radial profile is steady-state and non-coupled to the azimuthal direction, the integral over the radial direction causes all terms containing $f(r)$ to become constants. Thus we have essentially removed the radial direction and are left with a quasi-one-dimensional (in θ) Lagrangian that can be used to find the equation of motion for $A(\theta, t)$:

$$L_{1D} = \int_0^{2\pi} \mathcal{L}_{1D} d\theta,$$

where:

$$\mathcal{L}_{1D} = \frac{i}{2} C_1 (AA_t^* - A^* A_t) + C_2 |A|^2 + C_3 |A_\theta|^2 - \frac{s_1}{2} C_4 |A|^4 - \frac{s_2}{3} C_5 |A|^6, \quad (42)$$

where $C_i, i = 1, \dots, 5$ are the radial integrals of the steady-state profile $f(r)$ as defined in Eq. (25).

By evaluating the variational derivative of the action functional [13]:

$$\frac{\delta S}{\delta A^*} = \frac{\partial}{\partial t} \frac{\partial \mathcal{L}_{1D}}{\partial [A_t^*]} + \frac{\partial}{\partial \theta} \frac{\partial \mathcal{L}_{1D}}{\partial [A_\theta^*]} - \frac{\partial \mathcal{L}_{1D}}{\partial A^*} = 0, \quad (43)$$

yields the evolution equation for $A(\theta, t)$

$$i C_1 A_t = C_2 A - C_3 A_{\theta\theta} - s_1 C_4 |A|^2 A - s_2 C_5 |A|^4 A. \quad (44)$$

We now have a description of how a radially-frozen, azimuthally time-dependent solution will evolve in the CQNLS.

5.2 Stability Analysis

To study the AMS of vortex solutions to the CQNLS, we assume that they are separable into their radial and azimuthal parts, and that their radial profiles are steady-state, while their azimuthal structure is allowed to evolve in time. With these assumptions, we can use the azimuthal equation of motion of Eq. (44).

We first simplify Eq. (44) by applying the gauge transformation $A \rightarrow A \exp\left(-i\frac{C_2}{C_1}t\right)$ which eliminates the linear term proportional to A , and rescale time as:

$$t \rightarrow \frac{C_3}{C_1} t, \quad (45)$$

which eliminates C_1 from the equation, and moves C_3 to the nonlinear terms. Making these simplifications does not have an effect on our AMS results, as long as we keep the time rescaling in mind when computing growth rates. Our simplified azimuthal equation is now:

$$iA_t = -A_{\theta\theta} - s_1 \frac{C_4}{C_3} |A|^2 A - s_2 \frac{C_5}{C_3} |A|^4 A. \quad (46)$$

We now do a perturbation analysis to compute growth rates of a small complex modulated perturbation. We begin with an azimuthal ‘plane wave’ solution:

$$A(\theta, t) = e^{i(m\theta + \Omega' t)}, \quad (47)$$

where m is the topological charge of the vortex, and Ω' is the frequency of rotation of the complex phase. Since the amplitude of the plane wave can be absorbed into the $f(r)$ of Eq. (40), we set it here to 1 for simplicity. Inserting Eq. (47) into Eq. (46), yields the dispersion relation:

$$\Omega' = -m^2 + s_1 \frac{C_4}{C_3} + s_2 \frac{C_5}{C_3}. \quad (48)$$

We perturb Eq. (47) with a complex, time-dependent perturbation of the form:

$$A(\theta, t) = (1 + u(\theta, t) + iv(\theta, t)) e^{i(m\theta + \Omega' t)}, \quad (49)$$

where $|u|, |v| \ll 1$. After inserting this into Eq. (46), and using Eq. (48), we can separate the result into real and imaginary parts to get a system of coupled partial differential equations (PDEs) describing the evolution of the perturbation $u(\theta, t)$ and $v(\theta, t)$. The coupled PDEs can be simplified by setting ourselves on a rotating frame with angular velocity of $2m$ by rescaling time as $t \rightarrow t + \frac{1}{2m}\theta$. The simplified system of PDEs is

$$\begin{aligned} u_t &= -v_{\theta\theta} + [h.o.t], \\ v_t &= u_{\theta\theta} + \left(2s_1 \frac{C_4}{C_3} + 4s_2 \frac{C_5}{C_3}\right) u + [h.o.t], \end{aligned} \quad (50)$$

where [h.o.t] refers to higher order terms (which do not concern us as we are performing a linear stability analysis).

In order to study the AMS of the vortices, we need to obtain amplitude equations for the azimuthal modes. To do this, we first expand u and v in a discrete Fourier series:

$$u(\theta, t) = \frac{1}{2\pi} \sum_{K=-\infty}^{\infty} \hat{u}(K, t) e^{-iK\theta}, \quad v(\theta, t) = \frac{1}{2\pi} \sum_{K=-\infty}^{\infty} \hat{v}(K, t) e^{-iK\theta}, \quad (51)$$

where K is the mode number and where the amplitudes for each mode are given by:

$$\hat{u}(K, t) = \int_0^{2\pi} u(\theta, t) e^{iK\theta} d\theta, \quad \hat{v}(K, t) = \int_0^{2\pi} v(\theta, t) e^{iK\theta} d\theta. \quad (52)$$

Applying these transforms to Eq. (50) yields two coupled nonlinear ODEs describing the dynamics for the amplitudes of u and v for each mode.

If we linearize the ODEs and write them in matrix form, we get:

$$\frac{d}{dt} \begin{bmatrix} \hat{u} \\ \hat{v} \end{bmatrix} = \begin{bmatrix} 0 & K^2 \\ \left(2s_1 \frac{C_4}{C_3} + 4s_2 \frac{C_5}{C_3} - K^2\right) & 0 \end{bmatrix} \begin{bmatrix} \hat{u} \\ \hat{v} \end{bmatrix}. \quad (53)$$

The growth rates for each mode K can be found by finding the eigenvalues of Eq. (53):

$$\lambda_{1/2} = \pm \sqrt{K^2 \left(2s_1 \frac{C_4}{C_3} + 4s_2 \frac{C_5}{C_3} - K^2\right)}.$$

We have left explicitly s_1 and s_2 in our analysis until this point in order to keep results as general as possible. We now set them to $s_1 = +1$ and $s_2 = -1$ to correspond to the CQNLS which supports the bright vortices we are studying.

For the actual growth rates of our vortices, the time rescaling of Eq. (45) needs to be taken into account, and therefore the growth rates are:

$$\lambda_{1/2} = \pm \frac{C_3}{C_1} \sqrt{K^2 (K_{\text{crit}}^2 - K^2)}, \quad (54)$$

where K_{crit} is the critical value of K , below which all modes are stable and is defined as:

$$K_{\text{crit}} \equiv \sqrt{2 \frac{C_4}{C_3} - 4 \frac{C_5}{C_3}}. \quad (55)$$

We see that since all C -constants are positive, the minus sign in K_{crit} implies that K_{crit} could be less than 1 or purely imaginary. Both of these situations would result in the eigenvalues becoming purely imaginary, resulting in neutral stability (i.e. oscillations) of all azimuthal perturbation mode amplitudes.

The two criteria for stability are:

$$K_{\text{crit}} \in \Im : C_4 - 2C_5 < 0, \quad (56)$$

and

$$K_{\text{crit}} < 1 : C_4 - 2C_5 - \frac{C_3}{2} < 0. \quad (57)$$

In principle, the C -constants depend on m and Ω , as these two parameters determine the shape of the radial profiles. Therefore, it is possible to use Eqs. (56) and (57) to determine the critical stability value of the complex frequency $\Omega_{\text{st}}(m)$, above which, all vortices are azimuthally stable.

For the azimuthal modulationally unstable vortices, it may be useful to know the maximum growth rate and the mode that exhibits it. This is because when designing experiments, even an unstable vortex can be ‘stable enough’ for practical uses if the maximum perturbation growth rate is small. These can be found simply from Eq. (54) by taking its derivative equal to zero and solving for K , yielding the mode of maximum growth (and subsequently, the prediction of the number of filaments that the unstable vortices will break up into):

$$K_{\text{max}} = \sqrt{\frac{C_4 - 2C_5}{C_3}}. \quad (58)$$

We can then insert this value into Eq. (55), which yields a maximum growth rate of

$$\lambda_{\text{max}} = \frac{C_4 - 2C_5}{C_1}. \quad (59)$$

From this analysis, we have seen that by computing the radial integrals of the C -constants, we can predict the AMS of vortices. For testing our results, we will perform these integral computations numerically using our numerically-exact GN profiles from Sec. 4.3. However, as we saw in Sec. 4.3, our VA ansatz is a very good approximation to the true radial profiles. As such, we can use the VA to formulate analytical expressions for the C -constants, and thereby compute analytical stability predictions.

5.3 Analytical Stability Predictions Using VA Profile

Formulating AMS predictions using our VA ansatz is straightforward. We insert our VA expressions for r_c and Ω^* given by Eq. (29) into the already evaluated C -integrals of Eq. (26). These can then be used to form predictions of the growth rates of perturbation modes, the critical mode, and the maximum growth rate and the mode that exhibits it from Sec. 5.2. For example, the VA prediction for the growth rates of the perturbation modes comes out to be:

$$\lambda_{1/2}(K, m, \Omega^*) = \pm \frac{K}{m} \sqrt{(\Omega^* - G(\Omega^*)) \left[6\Omega^* + \frac{5\sqrt{3}}{4T} \sqrt{\Omega^*} - \frac{15}{8} - \frac{K^2}{m^2} (\Omega^* - G(\Omega^*)) \right]}. \quad (60)$$

The VA ansatz can be very helpful in predicting the critical value of $\Omega^*(m)$, above which all vortices are modulationally stable. (This is because the criteria given by Eq. (56) and (57) do not lend themselves to easy predictions for numerically computed C -constants).

By inserting the C -constants of Eq. (29) into the stability criteria, we get:

$$K_{\text{crit}} \in \Im : 6\Omega^* - \frac{15}{8} + \frac{5\sqrt{3\Omega^*}}{4T} = 0, \quad (61)$$

and

$$K_{\text{crit}} < 1 : \frac{m}{\sqrt{\Omega^* - G(\Omega^*)}} \sqrt{6\Omega^* - \frac{15}{8} + \frac{5\sqrt{3\Omega^*}}{4T}} - 1 = 0, \quad (62)$$

where T is defined as in Eq. (27), and as before $\Omega = G(\Omega^*)$.

What is interesting is that the criterion of Eq. (61) is independent of the charge m , while Eq. (62) is dependent on m . Also, we see that as $m \rightarrow \infty$, Eq. (62) \rightarrow Eq. (61).

If we solve Eq. (61) for Ω^* using a root finder, we get: $\Omega_{\text{st}^*}^* = 0.180400530$. We can insert this into Eq. (31) to yield the equivalent value for Ω which yields:

$$\Omega_{\text{st}^*}^{\text{va}} = 0.144320424. \quad (63)$$

Since this value is less than Ω_{max}^{2D} , this result predicts that azimuthally stable vortices exist for all charges m , as long as $\Omega > \Omega_{\text{st}^*}^{\text{va}}$.

We can also solve for Ω in the less restrictive criterion of Eq. (62) for various values of m . The results are shown in Fig. 9. We see that as one increases the vortex charge, the critical complex frequency $\Omega_{\text{st}}^{\text{va}}$ increases in value and eventually converges to $\Omega_{\text{st}^*}^{\text{va}}$. Thus, the stability window in Ω is higher for lower charges.

In Ref. [8], the authors also conclude that azimuthally stable vortices exist for all m , however according to their results, $\Omega_{\text{st}^*} = \Omega_{\text{max}}^{2D}$. Therefore the stability window shrinks towards 0 as $m \rightarrow \infty$. They estimate that the window shrinks at a rate proportional to $1/m^2$. This would preclude the hope of experimentally achieving a high-charge stable vortex, as the stability window would be too small.

According to our VA predictions, the value of Ω_{st} does increase as m increases (and as shown in Fig. 9, also does so proportional to $1/m^2$ compared with our constant $\Omega_{\text{st}^*}^{\text{va}}$). However, there is a substantial stability window for all charges m which remains constant for $m \rightarrow \infty$. If correct, this would open the door for achieving very high charge vortices experimentally. Unfortunately as we will see in Sec. 6, it appears that the predictions of Ref. [8] are more accurate.

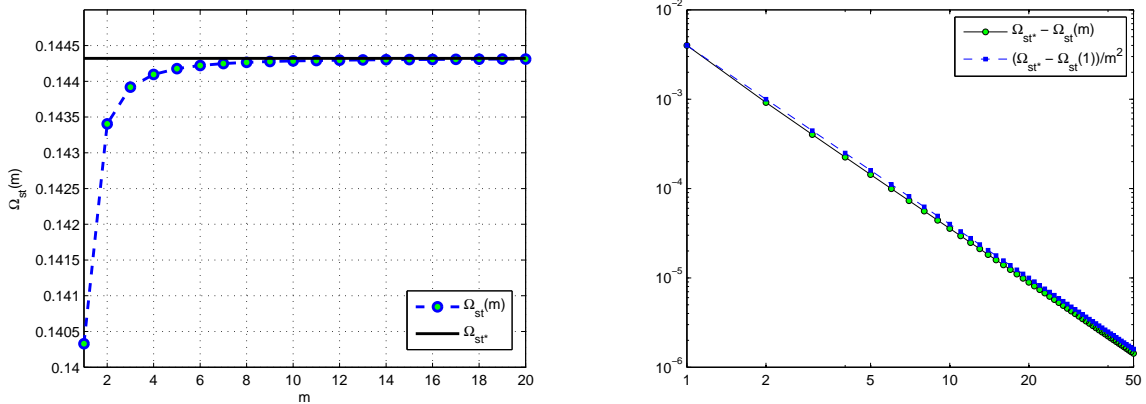


Figure 9: The critical value of the complex frequency $\Omega_{\text{st}}^{\text{va}}$ versus charge m according to our VA predictions (left). We see how as m increases, $\Omega_{\text{st}}^{\text{va}}(m) \rightarrow \Omega_{\text{st}}^{\text{va}*} < \Omega_{\text{max}}^{\text{2D}}$ implying that there exist azimuthally stable vortices for all charges. The rate of convergence is proportional to $1/m^2$ as shown in the figure on the right. We plot a $1/m^2$ line starting from our $m = 1$ computed value for comparison.

6 Azimuthal Modulational Stability - Numerical Results

Here we show the numerical predictions and results for AMS in vortices. We start by describing our integration method for the 2D CQNLS.

6.1 Numerical Method for Simulating Vortices in the 2D CQNLS

For our two-dimensional simulations, we will use both a polar-coordinate finite difference scheme as well as a Cartesian one. The polar grid makes computing the growth of individual perturbation modes very simple, and thus we use it to test our predictions for azimuthally unstable vortices. Using a polar grid forces one to use a smaller time step than one would need for an equivalent Cartesian grid scheme. Therefore, for testing the critical complex frequency Ω_{st} , we will use a Cartesian finite difference scheme (since testing for AMS stability will require us to run many very long simulations, and measuring the growth of individual perturbation modes is not important here).

For our polar-coordinate grid, the azimuthal direction is discretized with grid spacing of $\Delta\theta$, so that $\theta_j = j\Delta\theta$, $j = 1, \dots, J$ for $\theta \in [0, 2\pi]$ and the radial direction has spacing of Δr , so that $r_i = i\Delta r$, $i = 1, \dots, I$ for $r \in [0, r_{\text{max}}]$.

For the Cartesian grid, we discretize with equal spacing $\Delta x = \Delta y$, which we set to be equivalent to our Δr in the polar grid. In Fig. 10 we show an example of a vortex in our two coordinate grids. We denote the time step as Δt so that $t_n = n\Delta t$. Using this discretization, we have:

$$\Psi(r, \theta, t) = \Psi(r_i, \theta_j, t_n) \equiv \Psi_{i,j}^n,$$

or

$$\Psi(x, y, t) = \Psi(x_i, y_j, t_n) \equiv \Psi_{i,j}^n.$$

To integrate the two-dimensional CQNLS, we treat the time derivative separately from the spatial derivatives. Therefore we write Eq. (5) as:

$$\Psi_t = F(\Psi) = i(\nabla^2\Psi + |\Psi|^2\Psi - |\Psi|^4\Psi),$$

so that our time derivative scheme can evaluate F , which inside contains our spatial scheme, and the two

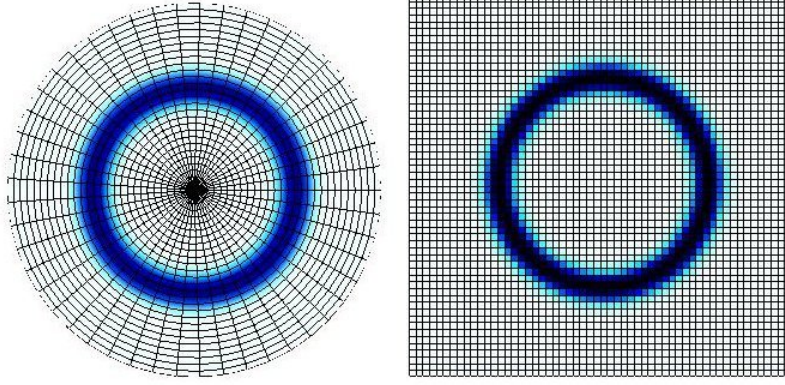


Figure 10: Example of displaying a vortex in the CQNLS in a polar (left) and Cartesian (right) grid. Shown is the modulus-squared of Ψ of a vortex of charge $m = 5$ and $\Omega = 0.16$. $\Delta x = \Delta y = \Delta r = 2$ and $\Delta\theta = \frac{2\pi}{50} \approx 0.125$.

are independent. For the time derivatives, we use the classic fourth order Runge-Kutta method [14]:

$$\Psi^{n+1} = \Psi^n + \frac{\Delta t}{6} (k_1 + 2k_2 + 2k_3 + k_4), \quad (64)$$

where

$$\begin{aligned} k_1 &= F(\Psi^n), & k_2 &= F(\Psi^n + \frac{\Delta t}{2}k_1), \\ k_3 &= F(\Psi^n + \frac{\Delta t}{2}k_2), & k_4 &= F(\Psi^n + \Delta tk_3), \end{aligned}$$

and $\Psi^n = \Psi_{i,j}^n \forall i, j$. We evaluate F at time n as:

$$F(\Psi_{i,j}) = i(\nabla^2 \Psi_{i,j} + |\Psi_{i,j}|^2 \Psi_{i,j} - |\Psi_{i,j}|^4 \Psi_{i,j}), \quad (65)$$

where $\Psi_{i,j} = \Psi_{i,j}^n$.

For evaluating the Laplacian in Eq. (65) in polar coordinates, we use the following form of the second order central difference scheme [15]:

$$\nabla^2 \Psi_{i,j} = \frac{1}{r_i} \frac{1}{\Delta r} \left(r_{i+\frac{1}{2}} \frac{\Psi_{i+1,j} - \Psi_{i,j}}{\Delta r} - r_{i-\frac{1}{2}} \frac{\Psi_{i,j} - \Psi_{i-1,j}}{\Delta r} \right) + \frac{1}{r_i^2} \frac{\Psi_{i,j+1} - 2\Psi_{i,j} + \Psi_{i,j-1}}{(\Delta\theta)^2}.$$

For the Cartesian grid, we use the classic second order finite difference:

$$\nabla^2 \Psi_{i,j} = \frac{\Psi_{i+1,j} - 2\Psi_{i,j} + \Psi_{i-1,j}}{(\Delta x)^2} + \frac{\Psi_{i,j+1} - 2\Psi_{i,j} + \Psi_{i,j-1}}{(\Delta y)^2}$$

In polar coordinates we must deal with three boundary conditions. The $\theta = 0, 2\pi$ line is the simplest to handle, for all that is necessary is to slightly alter the θ -derivative in the Laplacian in order for it to be periodic at $\theta = 0, 2\pi$:

$$\begin{aligned} j = 0, J & \rightarrow \frac{\Psi_{i,1} - 2\Psi_{i,0} + \Psi_{i,J-1}}{\Delta\theta^2}, \\ j = J - 1 & \rightarrow \frac{\Psi_{i,0} - 2\Psi_{i,J-1} + \Psi_{i,J-2}}{\Delta\theta^2}. \end{aligned} \quad (66)$$

For the $r = r_{\max}$ boundary, we use a Dirichlet condition of

$$\Psi(r = r_{\max}, \theta) = \Psi(r = 0, \theta) = 0. \quad (67)$$

For the $r = 0$ point, we could use the same Dirichlet condition, since by definition the center of the vortex is zero-valued. However, we have observed that for long simulations of stable and quasi-stable vortices, the vortex starts to drift from its position. Therefore, we need to evaluate the center point of our polar grid for which we use the following averaged extrapolation:

$$\Psi_{1,[1:J]}^{n+1} = \frac{1}{J} \sum_1^J \Psi_{2,j}^n.$$

At $r = r_{\max}$, we can only justifiably use Eq. (67) if we know that the wave function Ψ has a zero or nearly-zero value at the boundary. We can ensure this by using our VA profile ansatz to set our computational grid boundary. We solve for r in $f(r) = \epsilon$ where ϵ is some very small value (which we set to $\sqrt{\epsilon_{\text{mach}}}$, where $\epsilon_{\text{mach}} \sim 10^{-16}$ is machine precision). Doing this yields:

$$r_{\max}(\Omega^*, m, \epsilon) = \frac{1}{2\sqrt{\Omega^*}} \operatorname{arccosh} \left[\frac{4\Omega^* - \epsilon^2}{\epsilon^2 \sqrt{1 - 16/3 \Omega^*}} \right] + \frac{m}{\sqrt{\Omega^* - G(\Omega^*)}}. \quad (68)$$

For the Cartesian boundary conditions, we use Dirichlet conditions, setting our x_{\max} and y_{\max} equal to Eq. (68), and then setting $x_{\min} = -x_{\max}$ and $y_{\min} = -y_{\max}$.

In order to test our AMS predictions, we need a way to compute the growth of unstable perturbation modes.

6.2 Numerical Method for Computing AMS Results

In order to test for AMS of vortices in the CQNLS, we first test unstable vortices and see if our numerically computed theoretical predictions are accurate. To do this we test the growth rate of a single perturbed mode for different values of Ω and m . We choose to test the mode which we predict will exhibit the highest growth rate, as this will make it easier to see the growth and limit unwanted contributions from other nearby unstable modes.

To record the growth of a single mode, we set up our initial condition to perturb our chosen mode K along the azimuthal eigenvector direction [10]:

$$\Psi(r, \theta, 0; |K|) \equiv \Psi_{0;|K|} = f(r) \left[1 + \epsilon \left(\frac{K}{K_{\text{crit}}} + i \sqrt{1 - \left(\frac{K}{K_{\text{crit}}} \right)^2} \right) \cos(K\theta) \right] e^{im\theta}, \quad (69)$$

where ϵ is our perturbation amplitude which we typically set to 10^{-4} .

We let the simulation run until the predicted perturbation growth would grow to 1/2 of the initial wave function's modulus, which occurs at time:

$$t_{\text{end}} \approx \frac{N + \ln(0.5 \max|\Psi_0|)}{\lambda},$$

where λ is the predicted eigenvalue of the perturbed mode, and N is the magnitude of $\epsilon = 10^{-N}$.

While the simulation is running, we record the amplitude of the perturbation at each time step by extracting the azimuthal crest (which we denote as $\vec{\Psi}_{\text{crest}}$) at the center radius of the vortex, and then taking the difference between the maximum and minimum modulus value:

$$G(n) = |\max(\vec{\Psi}_{\text{crest}}^n) - \min(\vec{\Psi}_{\text{crest}}^n)|,$$

where n is the current time step. After the simulation is done, we calculate the growth rate over the simulation by computing the first derivative of $G(n)$ (using a central difference approximation):

$$G_{\text{rate}}(t) = \frac{d(\ln G(t))}{dt}.$$

We typically find that the perturbation growth takes some time to settle to a steady growth rate. Therefore we compute our average growth rate over a selected range of time where the growth rate seems most constant:

$$G_{\text{ave}} = \frac{1}{|t_e - t_s|} \sum_{t=t_s}^{t_e} G_{\text{rate}}(t) \Delta t,$$

where t_s is the start of our time range, and t_e is the end time. We illustrate this process in Fig. 11.

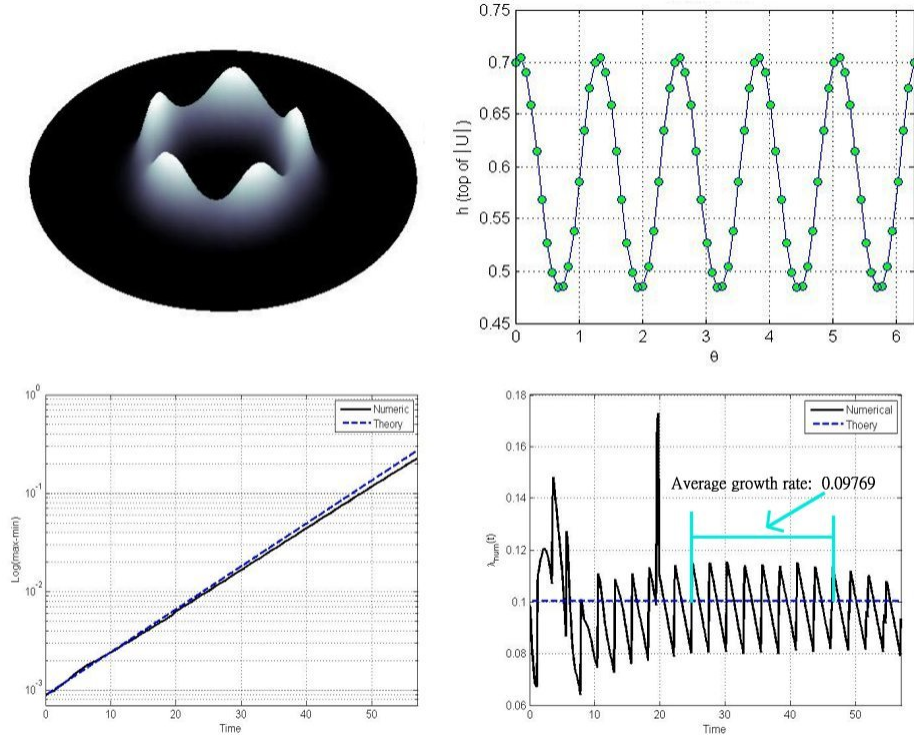


Figure 11: A typical example of computing the average growth rate of a perturbed azimuthal mode of a vortex in the CQNLS. The crest of the vortex (upper left) is extracted (upper right). The amplitude of the perturbation is measured over time (lower left), and then a central difference is taken of the result to yield the growth rate over time (bottom right). A time segment of the growth rate after it has settled is chosen and the average growth rate is computed. In this example, $\Omega = 0.1$, $m = 3$, $\epsilon = 0.001$, $\Delta r = 1$, $\Delta\theta = \lfloor 2\pi/100 \rfloor$, $\Delta t = 0.001$, and the most unstable mode is $K = 5$.

To study stable vortices [i.e. to determine the values of $\Omega_{\text{st}}(m)$] we simulate multiple vortices with Ω near the predicted values of $\Omega_{\text{st}}(m)$. Our method is to find an Ω value that results in an unstable vortex (and observe the break-up) and then show that the vortex solution at $\Omega + 0.001$ is stable by integrating it for at least twice the time necessary to show full break up in the original vortex. We do this for various charges. In Fig. 12 we show the initial and final vortices of this process for $m = 1$. Although in the figure we only show up to $t = 7000$ for the stable vortex, in subsequent simulations, we have integrated the same vortex to $t = 50,000$ and it still remains stable (although it starts to drift in its position on the grid — as can be seen on close inspection of the lower right panel of Fig. 12).

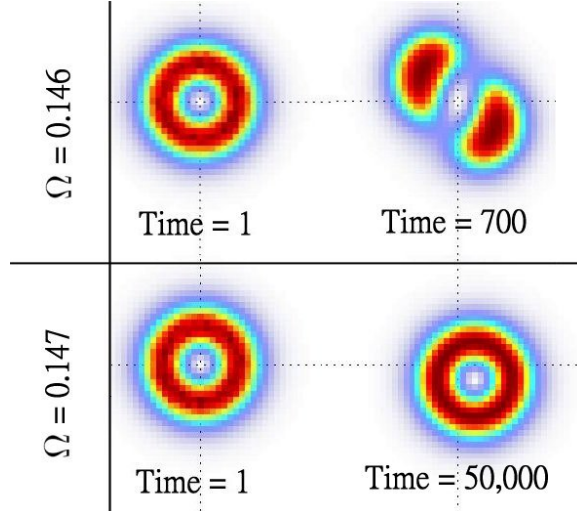


Figure 12: Example of numerically determining $\Omega_{\text{st}}(m)$ for $m = 1$. In this case a vortex with $\Omega_1 = 0.146$ (top left) is integrated with a random noise perturbation until it breaks up into filaments due to azimuthal instability (top right). We then integrate a vortex with $\Omega_2 = \Omega_1 + 0.001 = 0.147$ (bottom left) for ‘long enough’ to be satisfied that the vortex is stable — in this example for ten times the integration time of the $\Omega = 0.146$ vortex (bottom right). We then conclude that $\Omega_{\text{st}}(m = 1) \in [0.146, 0.147]$. We set $\Delta x = \Delta y = 1$, $\epsilon = 0.05$, and $\Delta t = 0.2$.

6.3 Numerical Predictions and Results

6.3.1 Unstable Vortices

In Fig. 13 we show our results for studying the AMS of vortices for charges $m = 1, \dots, 5$ and $\Omega \in [0.03, 0.14]$ using the method shown in Sec. 6.2.

In general, we see very good agreement for $m > 2$, however for high values of Ω our predictions become too low in each case. This implies that our predictions for $\Omega_{\text{st}}(m)$ will not be precise. To test this, we run long-time simulations of randomly perturbed vortices.

6.3.2 Stable Vortices

Here we show our results for finding $\Omega_{\text{st}}(m)$ using the method described in Sec. 6.2. For $m \in [1, 2, 3]$ we were able to notice the transition from unstable to stable vortices easily, but for $m > 3$ we found it very difficult to find a stable solution. Even for very large values of Ω , the vortex did not remain stable but eventually broke up. However, the dynamics of the break up is different than those observed for $m \in [1, 2, 3]$. The vortex exhibits snake-like oscillations in the radial direction and the shape of the ring gets warped, and then eventually breaks apart into non-symmetric irregular filaments. An example of this is given in Fig. 14. There is some evidence that this effect is due to numerical error. We have run further simulations with smaller time steps and smaller grid spacing and found that while the same effect occurs, it does so at a much later ‘real’ time in the simulation. Since this effect hinders our ability to simulate the vortices for extended time periods, we are not able to make any AMS predictions for vortices with $m > 3$.

In Table. 2 we display our VA predictions and simulation results for $m \in [1, 2, 3]$. We also show the predictions from previous studies for comparison. We see that most of the predictions for $m = 1$ are close to our numerical result. For $m = 2$ and $m = 3$, the predictions made by Ref. [8] are most accurate.

We have seen in Sec. 4.3 how our VA ansatz are extremely close to the numerically-exact vortex profiles. However, our AMS predictions made with the VA are not precise (although the scaling does match the scaling

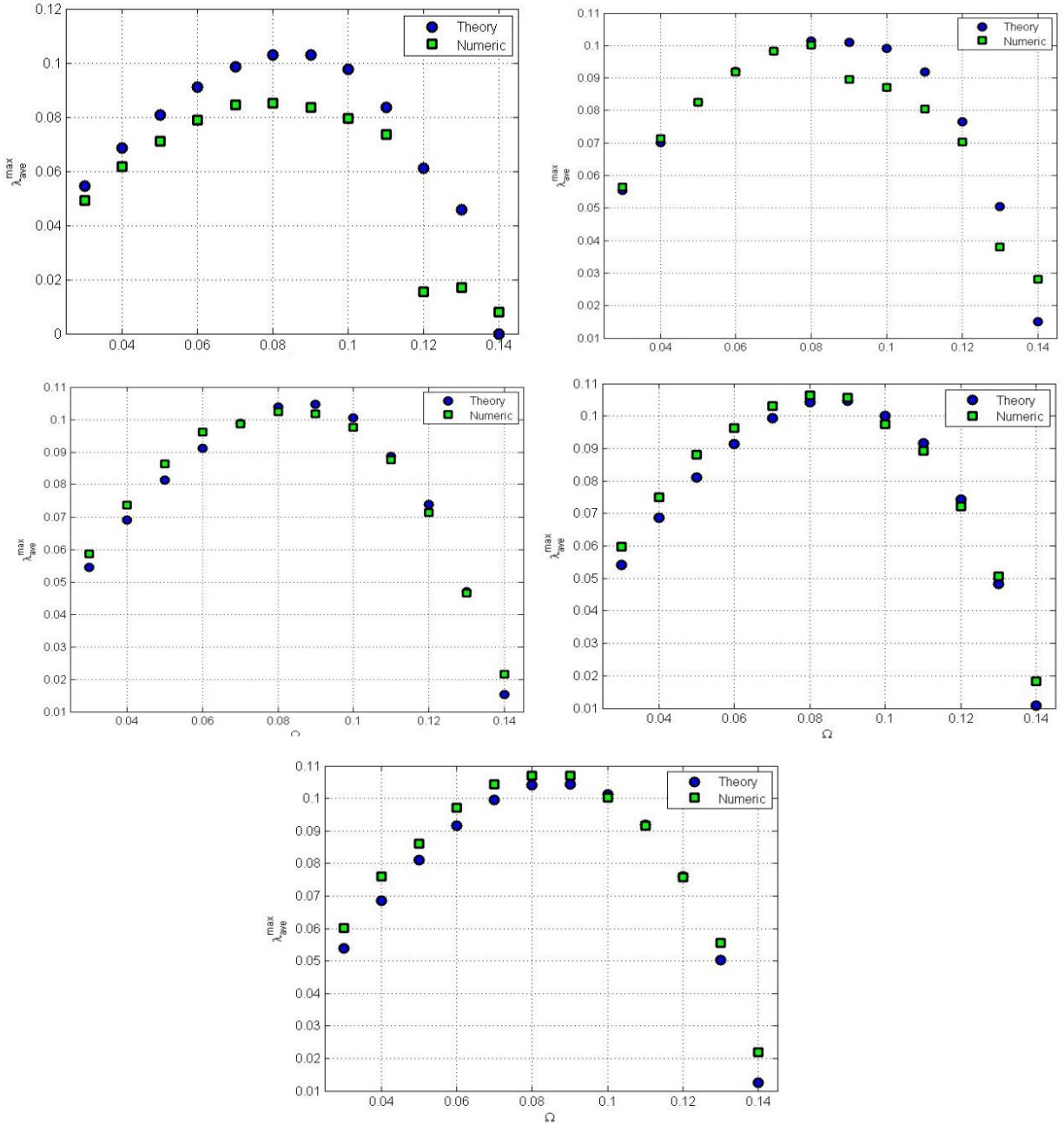


Figure 13: Theoretical predictions and numerical results of the growth rates of the azimuthal mode exhibiting the maximum growth rate for azimuthally unstable vortices of charges $m = 1, \dots, 5$ (left to right, top to bottom) in the CQNLS. For each value of $\Omega \in [0.03 : 0.01 : 0.14]$, we predicted the growth rates (shown as circles) using our numerically-exact profile for the C -integrals. We then run two-dimensional simulations of the vortex and use the method described in Sec. 6.2 to record the average growth rate (shown as squares). We set $\Delta r = 1$, $\Delta t = 0.001$, and $\Delta\theta = (2\pi)/(20 \max[m, K_{max}, 2])$. Overall, our predictions appear to match the numerical results very well.

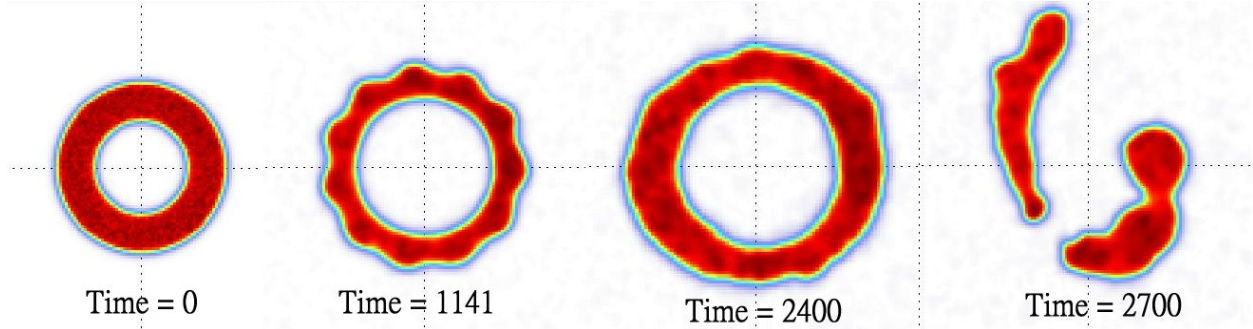


Figure 14: Example of shape distortion for a vortex of charge $m = 4$ and $\Omega = 0.18$ perturbed with a random perturbation of maximum size $\epsilon = 0.05$. Pictured is the modulus-squared of the wave function. We have set $\Delta r = 2$, $r_{\max} = 120$ and $\Delta t = 0.6$. We can easily see how the initial vortex shape becomes deformed and then breaks up irregularly.

Table 2: Comparison of predictions and numerical results for $\Omega_{\text{st}}(m)$. Our VA predictions are labeled ‘VA’, while our numerical results are labeled ‘NUM’. We also show predictions made by other studies. When no value has been computed or reported, we label the entry as ‘NP’. It seems that the predictions made in Ref. [8] are the most accurate compared to our simulations.

m	NUM	VA	Ref. [8]	Ref. [7]	Ref. [3]
1	0.147	0.1403	0.1487	0.16	0.145
2	0.162	0.1434	0.1619	0.17	NC
3	0.171	0.1439	0.1700	NC	NC
4	NC	0.1441	0.1769	NC	NC
5	NC	0.1442	0.1806	NC	NC

reported in Ref. [8]). Therefore, we conclude that the assumption that the vortex dynamics are completely separable is not a precise description but rather an approximation, and is the cause of our error.

7 Conclusion

We have studied the azimuthal modulational stability of vortices in the CQNLS using our method from Ref. [4]. By assuming a steady-state radial profile, we were able to derive a quasi-one-dimensional azimuthal equation of motion. Using a stability analysis in Fourier space we were able to form expressions to predict the azimuthal stability of the vortices. To compute the predictions, we developed an extremely accurate variational approach ansatz which we then refined into numerically-exact vortex profiles. We then ran full two-dimensional simulations of the CQNLS.

For azimuthally unstable vortices, our predictions of the maximum growth rate are fairly accurate over a wide range of the complex frequency (especially for vortices with charges greater than 2).

In studying stable vortices, our predictions of the critical complex frequency are not precise for charges greater than 1. From numerous simulations we do not believe this discrepancy to be a numerical error, but rather due to the assumption (required by our method of analysis) that the dynamics of the vortex are completely separable into radial and azimuthal parts.

From our two-dimensional simulations we were not able to find stable vortices with charges greater than 3. Such vortices, when predicted to be stable, become deformed in the radial direction eventually leading to break up. This effect could be caused by numerical errors, which requires further study.

References

- [1] S. Gatz and J. Herrmann. Soliton propagation and soliton collision in double-doped fibers with a non-kerr-like nonlinear refractive-index change. *Optics Letters*, **17**, 7 (1992) 484–486.
- [2] B. L. Lawrence and G. I. Stegeman. Two-dimensional bright spatial solitons stable over limited intensities and ring formation in polydiacetylene para-toluene sulfonate. *Optics letters*, **23**, 8 (1998) 591–593.
- [3] M. Quiroga-Teixeiro and H. Michinel. Stable azimuthal stationary state in quintic nonlinear optical media. *Journal of the Optical Society of America B*, **14**, 8 (1997) 2004–2009.
- [4] R. M. Caplan, R. Carretero-González, P.G. Kevrekidis and Q. E. Hoq. Azimuthal modulational instability of vortices in the nonlinear Schrödinger equation. *Optics Communications*, **282** (2009) 1399–1405.
- [5] I. Towers, A. V. Buryak, R. A. Sammut, B. A. Malomed, L.-C. Crasovan and D. Mihalache. Stability of spinning ring solitons of the cubic-quintic Nonlinear Schrödinger equation. *Physics Letters A*, **288** (2001) 292–298.
- [6] L. Crasovan, B. A. Malomed and D. Mihalache. Spinning solitons in cubic-quintic nonlinear media. *Pramana - journal of physics*, **57**, 5,6 (2001) 1041–1059.
- [7] B. A. Malomed, L.-C. Crasovan and D. Mihalache. Stability of vortex solitons in the cubic-quintic model. *Physica D*, **161** (2002) 187–201.
- [8] R. L. Pego and H. A. Warchall. Spectrally stable encapsulated vortices for Nonlinear Schrödinger equations. *Nonlinear Science*, **12** (2002) 347–394.
- [9] S. Cowan, R. H. Enns, S. S. Rangnekar and S. S. Sanghera. Quasi-soliton and other behavior of the nonlinear cubic-quintic Schrödinger equation. *Canadian Journal of Physics*, **64**, 3 (1986) 311–315.
- [10] R. M. Caplan. Azimuthal modulational instability of vortex solutions to the two dimensional nonlinear schrödinger equation. Master’s thesis, San Diego State University, 2008.
- [11] A. Desyatnikov, A. Maimistov and B. A. Malomed. Three-dimensional spinning solitons in dispersive media with the cubic-quintic nonlinearity. *Physical Review E*, **61**, 3 (2000) 3107–3113.
- [12] J. Nocedal and S. J. Wright. *Numerical Optimization*. Springer, New York, New York, 2 edition, 2006.
- [13] B. Malomed. Variational methods in nonlinear fiber-optics and related fields. *Progress in Optics*, **43** (2002) 71–193.
- [14] G. H. Golub and J. M. Ortega. *Scientific Computing and Differential Equations An Introduction to Numerical Methods*. Academic Press, San Diego, California, 2 edition, 1992.
- [15] J. C. Strikwerda. *Finite Difference Schemes and Partial Differential Equations*. Society for Industrial and applied Mathematics, Philadelphia, PA, 2 edition, 2004.